ACSNANO
www.acsnano.org
ARTICLE

Quantum Mode Selectivity of Plasmon-Induced Water Splitting on Gold Nanoparticles

Lei Yan, Fangwei Wang, and Sheng Meng*

Beijing National Laboratory for Condensed Matter Physics and Institute of Physics, Chinese Academy of Sciences, Beijing 100190, China

Collaborative Innovation Center of Quantum Matter, Beijing 100190, China

Supporting Information

ABSTRACT: **Plasmon induced water splitting is a promising research area with the potential for efficient conversion of solar to chemical energy, yet its atomic mechanism is not well understood. Here, ultrafast electron−nuclear dynamics of water splitting on gold nanoparticles upon exposure to femtosecond laser pulses was directly simulated using real time time-dependent density functional theory (TDDFT). Strong correlation between laser intensity, hot electron transfer, and reaction rates has been identified. The rate of water splitting is dependent not only on respective optical absorption strength, but also on the quantum oscillation mode of plasmonic excitation. Odd modes are more efficient than even modes, owing to faster decaying into hot electrons whose energy matches well the antibonding orbital of water. This finding suggests photocatalytic activity can be manipulated by adjusting the energy level of plasmon-induced hot carriers, through altering the cluster size and laser parameter, to better overlap adsorbate unoccupied level in plasmon-assisted photochemistry.**

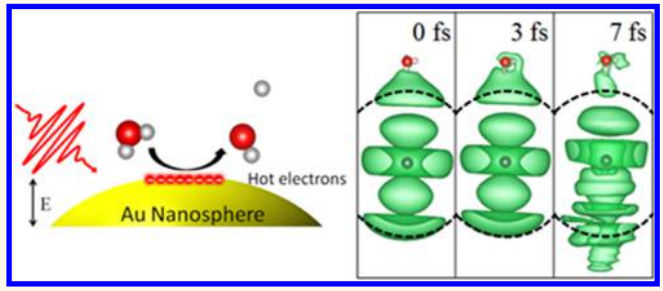

KEYWORDS: *photosplitting, ultrafast dynamics, hot electron, quantum plasmon mode, time-dependent density functional theory*

Plasmon driven photochemistry, as a route to concentrate and channel the energy of visible light into adsorbed molecules, has gained increasing attention thanks to its potential to drastically improve energy conversion technologies.[1,2] Examples of plasmon-induced chemical reactions include H_2/O_2 dissociation,[3−5] water splitting,[6−8] H_2 production from alcohol,[9,10] and hydrocarbon conversion.[11] The unique property of noble metal nanoparticles (NPs) to absorb and scatter light at specific wavelengths across a wide range of optical spectrum makes them excellent candidate for plasmon-assisted photochemistry.[2] The catalytic behavior of metal NPs with a diameter of 3−20 nm has been extensively investigated. A further decrease in NP diameter below 3 nm leads to unusual size dependence of reaction rate. For instance, TiO_2-supported Au NPs with a diameter of 1.87 nm possess the best activity for water reduction using visible light illumination among different NPs in the size range 1−6 nm.[12] Despite recent extensive efforts to address the extraordinary plasmonic catalytic behavior at reduced temperatures,[13−16] the atomic-level understanding is still lacking.

Solar water splitting is an essential step for artificial photosynthesis toward a sustainable energy future. Combining an oxide semiconductor with plasmonic metal nanostructures as cocatalyst for water splitting is prevalent in literature.[17−19] In this scenario, only hot electrons with sufficient energy to overcome the Schottky barrier can be collected by the conduction band of the semiconductor, and this bottleneck significantly limits the reaction efficiency. Recently, Robatjazi *et al.*[20] observed large photocurrents as a result of direct injection of hot electrons from plasmonic gold NP to molecules, driving solar water splitting in a Schottky-free junction. So far, such experiments show a rather low photocatalytic activity improper for practical use. The key to achieve significant efficiency improvement in this type of setup is strong light absorption and efficient carrier separation. Recent theoretical calculations start to attack the effect of size and shape of metal NPs on photocatalytic activity.[21,22] However, the microscopic mechanism of photocatalytic water splitting, especially its dynamic processes at the atomic scale, has not been illustrated.

Here, we investigate the atomic scale mechanism and real time dynamics of water splitting on Au NPs (diameter D = 1.6−2.1 nm) irradiated by femtosecond laser pulses, employing time-dependent density functional theory (TDDFT). Laser-induced hot electron generation and accumulation in the antibonding (AB) state of water are observed. By analyzing the dynamic charge distribution around water, we find a linear dependence of reaction rate on laser intensity, as a result of the

Received: March 16, 2016
Accepted: April 29, 2016
Published: April 29, 2016

DOI: 10.1021/acsnano.6b01840
ACS Nano 2016, 10, 5452−5458

linear correlation with hot electron transfer from Au NP to water. Surprisingly, wavelength-dependent water splitting rates are deviated from optical absorption spectra, suggesting a selectivity on plasmonic excitation mode. Odd mode is more effective in charge transfer than even mode, which is further attributed to the better overlap between the energy level of hot electrons and the AB state of water. These findings suggest that good energy alignment between hot electrons and adsorbate's empty states is crucial for achieving high efficiency in plasmon-driven reactions.

RESULTS AND DISCUSSION

We first investigate the dynamic response of water on Au NP (D = 1.9 nm) to laser field as shown in Figure 1c, which

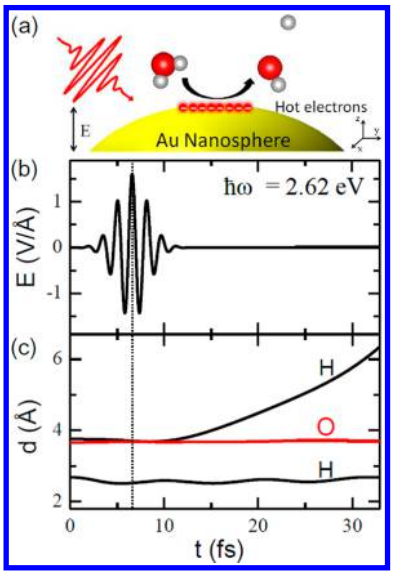

Figure 1. (a) The schematic showing plasmon-induced water splitting on Au nanosphere (D = 1.9 nm) under the laser field polarized in the z direction. (b) Time evolution of the applied field and (c) atomic distance d of water along the z direction to the Au surface. The vertical dotted line denotes the time t_0 = 6.6 fs at which laser field reaches its maximum strength.

displays time-dependent atomic distance d of water to the Au NP surface. The maximum field strength of laser pulse is set to E_{max} = 1.6 V/Å and frequency $\hbar\omega$ = 2.62 eV (Figure 1b). This frequency matches the plasmonic absorption peak at 2.62 eV calculated for the Au NP. For comparison, the major absorption peak at 2.60 eV is experimentally observed for Au NPs with the mean diameter of 1.9 nm embedded in alumina, in good agreement with our model.[23] From Figure 1c, we find that the O atom is almost static and the H atom pointing to the NP oscillates in a 10 fs period during the simulation timespan. The height of the other H first oscillates, then keeps increasing from d = 3.7 Å at t = 10 fs to d = 6.4 Å at t = 33 fs. The corresponding OH bond length increases from 1.12 to 2.84 Å. That is, water molecule splits into hydroxyl group (OH) and hydrogen (H) within 30 fs (time-evolved coordinates for water can be found in the Supporting Information). In contrast, for an isolated water molecule in the same laser field, two OH bonds oscillate continuously and never break. Therefore, we confirm that water splitting is mediated by plasmon excitation in the Au NP.

For simplicity, we define the rate of water splitting as the inverse of time needed for breaking the first OH bond, when its length reaches 2.0 Å. We find water splitting rate is strongly dependent on laser intensity, as shown in Figure 2a. Clearly, a

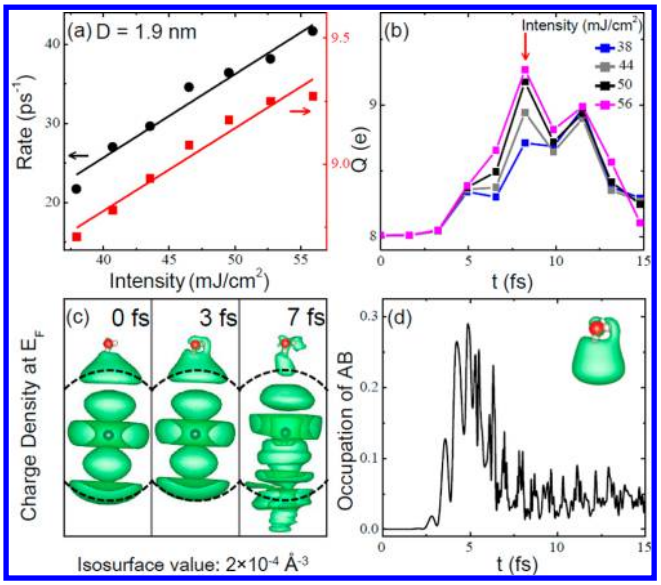

Figure 2. (a) The rate of water splitting (black circles) and total charge Q around water at t = 8.2 fs (red squares) as a function of laser intensity at a fixed frequency of 2.62 eV for Au NP (D = 1.9 nm). Linear fits to the data points are shown as the black and red lines. (b) Time evolution of charge Q around water for the same frequency 2.62 eV with varied laser fluences 38, 44, 50, and 56 mJ/cm^2. These values give the E_{max} of 1.4, 1.5, 1.6, and 1.7 V/Å, respectively. The vertical arrow specifies the time t = 8.2 fs. (c) Snapshots of the simulated time evolution of charge density at the Fermi level. The gray dot denotes the center of the NP, and the dashed line indicates the NP surface. (d) Time-evolved occupation of AB state of water under the laser with E_{max} = 1.6 V/Å and $\hbar\omega$ = 2.62 eV. Inset is the charge density of AB orbital of the adsorbed water.

linear fit of reaction rates on the laser intensity indicates that this is a one photon process.[24] In experiments, this linear relationship has been observed in the ethylene epoxidation on Ag nanocubes[25] and hydrogen dissociation on Au NPs.[3]

To illustrate the nature of photoexcitation, the dynamic charge Q around water is calculated in Figure 2b. The charge Q is calculated by integrating total charge density in a sphere with a radius of 4.5 Å around water. Initially, Q = 8.0e for all cases of different laser intensity. At t = 8.2 fs, Q increases to a maximum of 8.7−9.3e for laser intensity in the range of 38−56 mJ/cm^2, indicating that 0.7−1.3e is transferred from Au NP to H_2O. We find that the maximum charge Q is also linearly dependent on laser intensity, closely following the trend of reaction rates, as plotted in Figure 2a. Namely, increasing laser intensity results in increased charge transfer from Au NP to water, and subsequent rate enhancement for water splitting. In addition, below a critical laser fluence, no charge transfer occurs, and water does not split.[26] We also examined the time-dependent charge density at the Fermi level E_F (Figure 2c). Initially (t = 0 fs), there is almost no electron distributed on the water. At t = 3 and 7 fs, a small part of electrons indeed transfer from Au NP to water, implying state hybridization between Au NP and water. Thus, we provide direct evidence that water photo-splitting on Au NP is induced by photoelectric conversion.

DOI: 10.1021/acsnano.6b01840
ACS Nano 2016, 10, 5452−5458

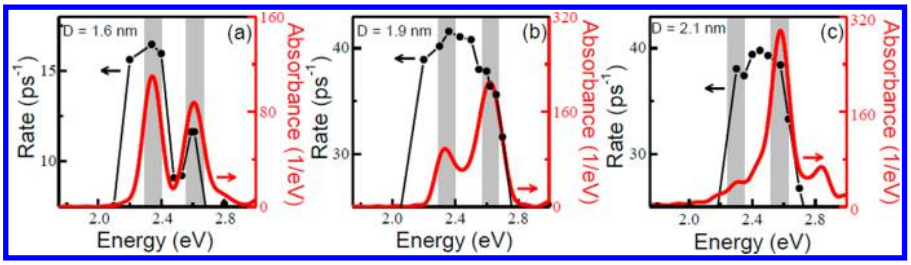

Figure 3. Water splitting rates (black dots) on Au NP with the diameter D of 1.6 nm (a), 1.9 nm (b), and 2.1 nm (c), for the pulse shape shown in Figure 1b with varied laser frequency. The connected line is the guide to eyes. Corresponding absorption spectrum (red lines) of Au NP to an impulse excitation in the z direction is superimposed for comparison.

To gain further insights into reaction mechanism of plasmon-induced water splitting, we display time-evolved occupation of AB state of water in Figure 2d. We calculate the localized density of states (LDOS) of water by projecting onto a sphere centered the oxygen atom with the radius of 2 Å. Then, we find the local orbital with the AB character of water and label it as the AB state of water. The occupation coherently oscillates following laser field and keeps increasing to 0.3 (~0.6 electrons) before t = 5 fs. Increased laser intensity after t = 5 fs leads to electron scattering and phase shifts.[27] After that, the occupation starts to decline and a dephasing process occurs. These observations provide compelling evidence that the occupation of AB orbital in water on Au NP leads to water splitting.

Further evidence implicating plasmon-induced reaction can be drawn from wavelength-dependent photocatalytic rates, shown in Figure 3. For the Au NP with D = 1.6 nm, the absorption spectrum shows double peaks due to quantum size effect. Similar splitting of absorption spectrum has been observed experimentally for thiol-protected Au_{25} clusters,[28] and Ag NP with diameters ranging from 20 down to 1.7 nm.[29] No matter for Au NP with or without water adsorbed, low-energy absorption peak always exists. According to the previous analysis of electronic transition,[30,31] both major absorption peaks are plasmonic. The existence of the two peaks may be due to the unique structure of the model system or the jellium electronic structure, which might be washed out in experiments where a huge number of particles with slightly different shapes are probed. Reaction rates also exhibit two major peaks, closely following the absorption spectrum. The reaction rate of 16 ps^{-1} for the plasmon excitation mode at $\hbar\omega$ = 2.34 eV is higher than 12 ps^{-1} for the mode at $\hbar\omega$ = 2.61 eV, in coincidence with corresponding absorption intensity, which has a ratio of 1.25:1. Therefore, in the case of D = 1.6 nm, water splitting rate compares well with absorption spectrum, in good agreement with previous experimental measurements.[2−8]

However, surprising contrast in reaction rate and photo-absorption is found for Au NP of larger size. For Au NP with a diameter D = 1.9 nm, the intensity for absorption at resonance frequency $\hbar\omega$ = 2.62 eV is almost doubled compared to that for $\hbar\omega$ = 2.36 eV. The reaction rate with laser frequency $\hbar\omega$ = 2.62 eV, however, is only 36 ps^{-1}, even smaller than the rate of 42 ps^{-1} at $\hbar\omega$ = 2.36 eV (black dots in Figure 3b). Again, for Au NP with D = 2.1 nm, the reaction rate (38 ps^{-1}) at $\hbar\omega$ = 2.63 eV, where the maximum absorption is reached, is almost same with that (38 ps^{-1}) at $\hbar\omega$ = 2.30 eV with only weak absorption (Figure 3c). In the recent experiment using aluminum nanocrystals as a plasmonic photocatalyst for hydrogen dissociation, maximum HD production is also observed at illumination wavelengths around 800 nm, even though its absorption peak is smaller than the plasmonic mode at around 460 nm.[32] However, the authors assigned the low-energy peak to the Al interband transition, not a plasmon. Also, the separation between the peaks is about 1.3 eV, much larger than ~0.3 eV in the present model.

Above simulations strongly suggest that the rate of water splitting depends not only on optical absorption of Au NP, but also on its plasmonic excitation mode. To understand why plasmonic mode would affect the rate of water splitting, we display Fourier transform of induced charge density for both modes in Figure 4. Take the Au NP with diameter D = 1.9 nm

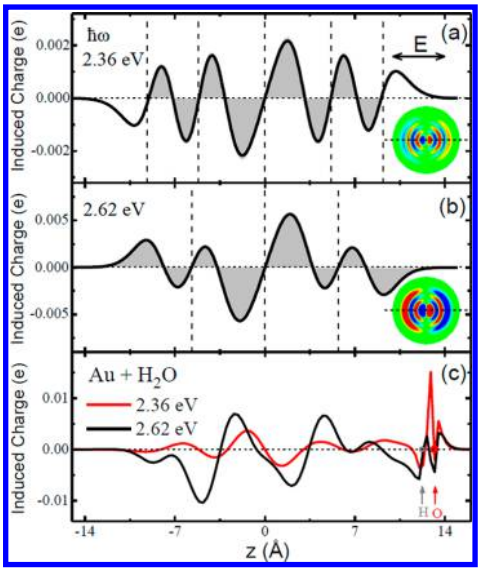

Figure 4. Fourier transform of induced charge density for Au NP (D = 1.9 nm) at two plasmon resonances 2.36 eV (a) and 2.62 eV (b), and for AuNP + H_2O (c) at the resonant frequency 2.36 eV (red line) and 2.62 eV (black line), to an impulse excitation along the z axis. Inset shows corresponding induced density projected into the xz plane with the dotted line directing the z axis. The dashed line in (a) and (b) is for partition of one oscillation period. The red and gray dots in (c) specify the position of oxygen and hydrogen atom, respectively. The second hydrogen atom is at the same distance as the oxygen atom.

as an example. For the mode at $\hbar\omega$ = 2.36 eV, there are two oscillating periods and one-half period from the NP center to both sides (Figure 4a); therefore, the oscillation period n is odd (n = 5). For the mode at $\hbar\omega$ = 2.62 eV, there are only two oscillating periods from the center to both sides (Figure 4b), and this is even-period plasmon excitation (n = 4). Upon water adsorption, we find that the odd mode indeed induces more electrons around water than the even mode (Figure 4c), due to

DOI: 10.1021/acsnano.6b01840
ACS Nano 2016, 10, 5452−5458

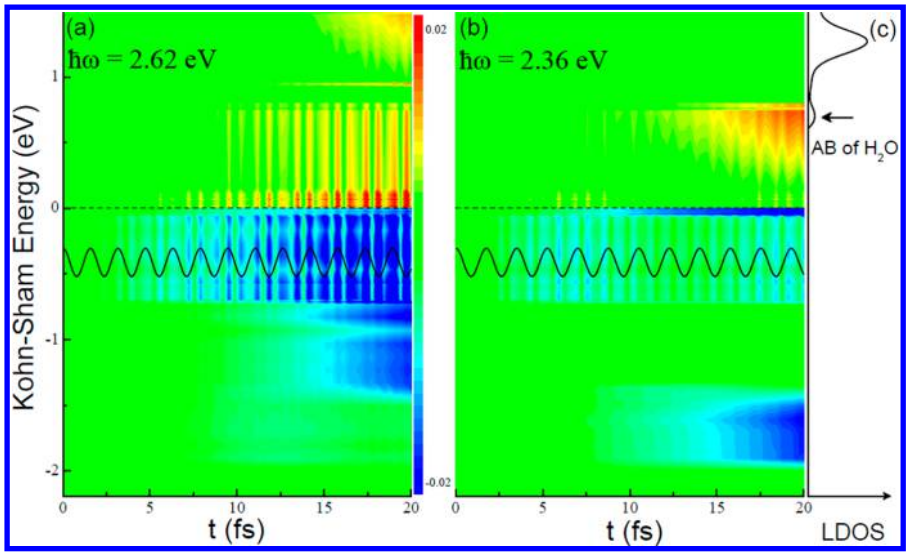

Figure 5. Time-evolved changes in the occupation of KS states for Au NP (D = 1.9 nm) when driven by continuous plane-wave laser at the frequency of 2.62 eV (a) and 2.36 eV (b) with an amplitude of 0.01 V/Å. Black line denotes laser field oscillations. (c) Calculated localized density of states (LDOS) of water. Horizontal dashed line denotes the Fermi level.

net electrons in the half period of the odd mode strongly couple to water.

The same phenomenon is observed for the Au NP with D = 1.6 nm (Figure S1). However, for the Au NP with D = 1.6 nm, there is a slightly larger induced charge at the odd mode, but the effect is much less pronounced than that for NP with D = 1.9 nm. We also examine the NP with D = 2.1 nm, and find that the mode at 2.63 eV seems to induce more electrons around water than that at 2.30 eV in Figure S2. Yet, the reaction rates for both modes are almost the same. Therefore, we would explore further other mode-associated mechanisms affecting the reaction rates.

To further understand photoexcitations associated with odd and even modes, we analyze time-evolved change in the occupation of KS states, when Au NP (D = 1.9 nm) is driven by plane-wave laser at a resonant energy of 2.36 and 2.62 eV, respectively. The occupation of KS states is calculated by projecting the time-dependent KS state onto ground state. For $\hbar\omega$ = 2.62 eV, there exist strong oscillations in the occupation of states near the Fermi level (Figure 5a), which is designated as electron "sloshing",[33] and electron excitations from deep states with the energy at −1.43 to about −0.72 eV to the states at 1.40−1.50 eV, called "inversion" motion.[33] The "sloshing" behavior around Fermi level results in oscillations in the charge density near the NP surface,[34] while "inversion" is responsible for plasmon decaying into hot electrons and hot holes.[35] Compared with even mode excitation at $\hbar\omega$ = 2.62 eV, the variation in the occupation of KS orbitals for the odd mode at $\hbar\omega$ = 2.36 eV is minor, and there mainly exhibits electron inversion from the orbitals between −1.90 eV and −1.50 eV to those at 0.58−0.79 eV (Figure 5b). For the peak at 2.62 eV, the contribution mainly comes from electron transitions from the KS orbitals between −1.43 eV and −0.72 eV to those at 1.40−1.50 eV.

We calculate the localized density of state of water on Au NP, as shown in Figure 5c. The AB state of water appears at the energy of 0.64 eV, overlapping well with the KS orbitals of Au NP which are newly partly occupied upon excitation at $\hbar\omega$ = 2.36 eV. The energy match promotes resonant charge transfer from Au NP to water. However, for the even mode at $\hbar\omega$ = 2.62 eV, orbital occupation near the Fermi level strongly oscillates, and there is no net electron accumulation in these orbitals. Specifically, we show in Figure 6 all the transition

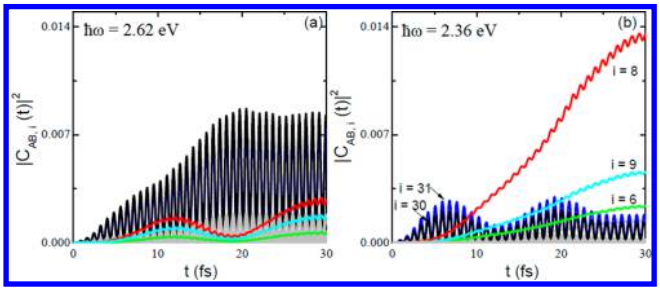

Figure 6. Time-evolved coefficient $|C_{AB,i}(t)|^2$ from all the occupied states i to AB state for Au NP (D = 1.9 nm), when driven by continuous plane-wave laser at the frequency of 2.62 eV (a) and 2.36 eV (b) with an amplitude of 0.01 V/Å. The index i denotes the state by the order of increasing orbital energy. A few important orbitals which make major contributions to density change are labeled, and all other transitions are shown as gray lines.

coefficients $|C_{AB,i}(t)|^2$, defined as the time-dependent occupied KS orbital $|i(t)\rangle$ projected onto the initial AB state. The so-called "initial AB state" is the AB orbital corresponding to original geometry at t = 0. Two distinct types of transitions can be clearly observed: one type is high-frequency synchronized oscillations constituting plasmon excitation (for example, for i = 30, 31); the other shows smooth gradual amplitude increase corresponding to hot-electrons generation by plasmon decay (for example, for i = 6, 8, 9).[35] Clearly, the former type of oscillations dominates for the excitation at $\hbar\omega$ = 2.62 eV, while the latter dominates for $\hbar\omega$ = 2.36 eV, namely, more hot electrons are generated and accumulated into the AB orbital at $\hbar\omega$ = 2.36 eV.

For Au NPs with D = 1.6 and 2.1 nm, we find the same trend: hot electrons are generated and accumulated *via* resonant plasmon decay into the KS orbitals whose energy level overlaps better with the AB orbital of water, resulting in higher water splitting rates (Figures S3 and S4). We stress that the time-evolved changes in the KS states above is for the Au

DOI: 10.1021/acsnano.6b01840
ACS Nano 2016, 10, 5452−5458

NP without the water present. To further judge the plasmon decay cascade, we have calculated the time-evolved changes in the KS states for the Au NP (D = 2.1 nm) with water present shown in Figure S5. We find that, no matter for the Au NP with and without the water present, plasmon starts to decay into hot electrons at the time t = 20 fs. Thus, we can infer that plasmon decays by directly charge transfer from Au NP to water. We also note that more hot electrons are generated for D = 1.9 nm at the frequency of 2.36 eV than those for D = 2.1 nm at the frequency of 2.30 eV. Thus, Au NPs for D = 1.9 nm is more effective for water splitting as shown in Figure 3. For photodecomposition of ethyl chloride on Ag NPs, the energy alignment of excited electrons and unpopulated adsorbate levels is also central to induce efficient photochemical reactions.[36]

We have also checked the effects for a variation in water orientation. For the water molecule parallel to the surface of Au NP (D = 1.9 nm), the reaction rate of 28 ps^{-1} at $\hbar\omega$ = 2.36 eV (odd mode) is also larger than that of 27 ps^{-1} at $\hbar\omega$ = 2.62 eV (even mode) under the same laser illumination as in the Figure 3. Compared with the upright water orientation in Figure 3, the reaction rate is decreased due to the unfavorable water dipole alignment. In addition, we also find that the mode at 2.36 eV has a better energy match with the AB of water than the mode at 2.62 eV (Figure S6), the same phenomenon as that shown in Figure 5. Therefore, the perfect energy match between hot electrons generated from plasmon decay and the AB state of water is the major reason for the enhanced water splitting reactivity in odd mode excitation.

CONCLUSIONS

On the basis of above analysis, we provide a real-time picture of reaction mechanism for direct plasmon-driven water splitting on Au NP. Plasmon of Au NP is initially optically excited, leading to electron density oscillations around the Fermi level and subsequent low energy electron−hole excitations. In other words, plasmon decays into resonant hot electrons and holes, where hot electrons transfer to the water and holes are kept in the Au NP. Above processes occur simultaneously at a time scale of 10−20 fs and the excited electrons with sufficient energy directly transfer to the AB orbital of water, subsequently leading to water splitting. Thus, we present atomic scale insights into an ultrafast plasmon decay pathway, chemical interface damping (CID), to represent direct electron injection from metal into the adsorbate states.[24,37−39] The CID mechanism plays an important role in the field of photochemical catalysis on plasmonic metallic nanostructures.[40] For example, it results in accelerated rates of chemical decomposition of a probe molecule on optically excited Ag nanocube,[41] and selectivity control in CO oxidation on the sub-5-nm Pt nanoparticle.[31] Recently, Wu *et al.*[42] also demonstrated the ultrafast hot-electron transfer from gold tips to cadmium selenide nanorods on the time scale of ∼20 ± 10 fs. Thus, the CID mechanism is potentially a general phenomenon at metal/molecule and metal/semiconductor interfaces.

In above simulations, we have not included liquid water background due to the heavy computational loads in real time TDDFT dynamic simulations. We note that the dissociation process would likely be significantly influenced by water medium. First, the intensity of optical absorption would decrease because of optical scattering of liquid water, and absorption peak would shift due to the interaction between water molecules and gold NPs. Take the Au_{20} cluster enclosed with 52 water molecules as an example. There indeed exists excitation energy shift and peak splitting in optical absorption spectrum when the gold cluster is embedded in the water medium (Figure S7). Second, the reaction products would be also altered. It is no longer simply the H desorbed from the Au−water cluster leaving behind an OH. In the model of $Au_{20}(H_2O)_{52}$, a water molecule first traps a H atom from the neighboring water molecule, forming a H_3O^+ ion, then releases a H atom of its own to other water molecules. The reaction barrier is thus lowered by the assistance of hydrogen bonds between water molecules in this process. Therefore, we estimate the reaction rate would increase and laser intensity required for reaction would decrease in the presence of aqueous medium. The present analysis concerns only the initiating steps in water photosplitting reactions, and does not address O_2 and H_2 evolution, which would require sequential excitations. The endothermic nature of the overall reaction favors that H + OH likely occur before the sequential reaction steps. This is important because it has not been shown that the complete reaction for water splitting can be driven on the surface of Au by plasmonic excitation, without Schottky barriers and cocatalysts.[7,18]

In conclusion, by directly looking into dynamic processes using TDDFT, we illustrate the mechanism of plasmon-induced water splitting at atomic scale and identify the unexpected mode-selectivity in water splitting rate on small metal NPs. The latter is ascribed to direct plasmon-induced charge transfer, which has a good energy overlap with water's antibonding state. In the experiment of hydrogen dissocaition on aluminum nanocrystals, energy alignment of hot electrons generated from plasmon decay with AB orbitals of hydrogen also facilitates this reaction.[32] Thereby, charge-transfer enhancement by better energy overlap between plasmon-induced carriers and the adsorbate's unpopulated state is crucial for plasmon-enhanced reactions. On this regard, we could adjust laser parameters and nanoparticle size to control electronic energy alignment and dynamics to dramatically improve energy conversion efficiency in plasmon-assisted photochemistry.

METHODS

All calculations are performed with real space TDDFT code OCTOPUS,[43] where atoms are treated with norm-conserving pseudopotentials. We use a jellium sphere with electron density r_s = 4.5 au to simulate the Au NP with a diameter D = 1.6−2.1 nm. This approximation is commonly used in literature since it captures the most important properties of metallic NPs.[44−47] The electron−nuclear interactions are described by the Troullier−Martins pseudopotentials[48] in the local density approximation (LDA)[49] with the real-space grid point separation of 0.3 Å. Electron−ion dynamics is treated with the Ehrenfest scheme controlled at the electronic propagation time step.[50] In electron dynamic simulations, Kohn−Sham (KS) eigenstates are propagated with a time-dependent Hamiltonian, representing a continuous plane-wave or Gaussian-wave laser field of constant frequency. The system is evolved for >10 000 steps with a time step of 0.003 fs and temperature fluctuating at around 300 K. A delta function for electromagnetic pulse is also used in order to obtain optical absorption spectrum.[51,52]

The geometry for a water molecule adsorbed on Au NP is shown in Figure 1a. Water molecule is initially placed 3.66 Å away from NP surface with one hydrogen (H) atom pointing toward the NP. The stable geometry in the ground state molecular dynamics simulation was chosen as the starting structure for the TDDFT simulations. Similar structures were reported for water adsorption on small gold clusters.[53] External laser field polarized in the z direction, which runs

DOI: 10.1021/acsnano.6b01840
ACS Nano 2016, 10, 5452−5458

through the center of nanosphere (set as $z = 0$) and the oxygen (O) atom, is shaped by a Gaussian wave packet (Figure 1b)

$$E(\omega, t) = E_{max} \exp\left[-\frac{(t - t_0)^2}{2\tau^2}\right] \cos(\omega t - \omega t_0 + \varphi)$$

where the phase φ is set to zero and parameter τ is 1.6 fs. Laser field reaches the maximum intensity E_{max} at the time t_0 = 6.6 fs. We also tested laser pulses with longer duration which essentially result in the same trends. Photoexcitation of metal NPs by few-cycle pulses has been achieved experimentally, and dynamics of local field enhancement by silver NPs is demonstrated.[54]

ASSOCIATED CONTENT

Supporting Information

The Supporting Information is available free of charge on the ACS Publications website at DOI: 10.1021/acsnano.6b01840.

Coordinates of the significant structures under the laser pulse; induced density of plasmonic mode and time-evolved changes in the occupation of Kohn−Sham states for Au NPs with D = 1.6 and 2.1 nm; optical absorption spectrum for gold cluster embedded in the water medium; calculation detail for transition coefficients (PDF)

AUTHOR INFORMATION

Corresponding Author

*E-mail: smeng@iphy.ac.cn.

Notes

The authors declare no competing financial interest.

ACKNOWLEDGMENTS

We acknowledge helpful discussions with S.W. Gao, and financial support from the "973" Project of China (No.2012CB921403), NSFC (Grant Nos. 11474328, 11290164, and 11222431), and "Strategic Priority Research Program B" of the CAS (No. XDB070301).

REFERENCES

(1) Brongersma, M. L.; Halas, N. J.; Nordlander, P. Plasmon-Induced Hot Carrier Science and Technology. *Nat. Nanotechnol.* **2015**, *10*, 25−34.

(2) Linic, S.; Christopher, P.; Ingram, D. B. Plasmonic-Metal Nanostructures for Efficient Conversion of Solar to Chemical. *Nat. Mater.* **2011**, *10*, 911−921.

(3) Mukherjee, S.; Libisch, F.; Large, N.; Neumann, O.; Brown, L. V.; Cheng, J.; Lassiter, J. B.; Carter, E. A.; Nordlander, P.; Halas, N. J. Hot Electrons Do the Impossible: Plasmon-Induced Dissociation of H_2 on Au. *Nano Lett.* **2013**, *13*, 240−247.

(4) Mukherjee, S.; Zhou, L.; Goodman, A. M.; Large, N.; Ayala-Orozco, C.; Zhang, Y.; Nordlander, P.; Halas, N. J. Hot-Electron-Induced Dissociation of H_2 on Gold Nanoparticles Supported on SiO_2. *J. Am. Chem. Soc.* **2014**, *136*, 64−67.

(5) Christopher, P.; Xin, H.; Marimuthu, A.; Linic, S. Singular Characteristics and Unique Chemical Bond Activation Mechanisms of Photocatalytic Reactions on Plasmonic Nanostructures. *Nat. Mater.* **2012**, *11*, 1044−1050.

(6) Shi, Y.; Wang, J.; Wang, C.; Zhai, T. T.; Bao, W. J.; Xu, J. J.; Xia, X. H.; Chen, H. Y. Hot Electron of Au Nanorods Activates the Electrocatalysis of Hydrogen Evolution on MoS_2 Nanosheets. *J. Am. Chem. Soc.* **2015**, *137*, 7365−7370.

(7) Lee, J.; Mubeen, S.; Ji, X.; Stucky, G. D.; Moskovits, M. Plasmonic Photoanodes for Solar Water Splitting with Visible Light. *Nano Lett.* **2012**, *12*, 5014−5019.

(8) Ingram, D. B.; Linic, S. Water Splitting on Composite Plasmonic-Metal/Semiconductor Photoelectrodes: Evidence for Selective Plasmon-Induced Formation of Charge Carriers near the Semiconductor Surface. *J. Am. Chem. Soc.* **2011**, *133*, 5202−5205.

(9) Murdoch, M.; Waterhouse, G. I. N.; Nadeem, M. A.; Metson, J. B.; Keane, M. A.; Howe, R. F.; Llorca, J.; Idriss, H. The Effect of Gold Loading and Particle Size on Photocatalytic Hydrogen Production from Ethanol over Au/TiO_2 Nanoparticles. *Nat. Chem.* **2011**, *3*, 489−492.

(10) Seh, Z. W.; Liu, S.; Low, M.; Zhang, S. Y.; Liu, Z.; Mlayah, A.; Han, M. Y. Janus $Au-TiO_2$ Photocatalysts with Strong Localization of Plasmonic Near-Fields for Efficient Visible-Light Hydrogen Generation. *Adv. Mater.* **2012**, *24*, 2310−2314.

(11) Hou, W.; Hung, W. H.; Pavaskar, P.; Goeppert, A.; Aykol, M.; Cronin, S. B. Photocatalytic Conversion of CO_2 to Hydrocarbon Fuels *via* Plasmon-Enhanced Absorption and Metallic Interband Transitions. *ACS Catal.* **2011**, *1*, 929−936.

(12) Gomes Silva, C.; Juárez, R.; Marino, T.; Molinari, R.; García, H. Influence of Excitation Wavelength (UV or Visible Light) on the Photocatalytic Activity of Titania Containing Gold Nanoparticles for the Generation of Hydrogen or Oxygen from Water. *J. Am. Chem. Soc.* **2011**, *133*, 595−602.

(13) Turner, M.; Golovko, V. B.; Vaughan, O. P. H.; Abdulkin, P.; Berenguer-Murcia, A.; Tikhov, M. S.; Johnson, B. F. G.; Lambert, R. M. Selective Oxidation with Dioxygen by Gold Nanoparticle Catalysts Derived from 55-atom Clusters. *Nature* **2008**, *454*, 981−983.

(14) Qian, K.; Sweeny, B. C.; Johnston-Peck, A. C.; Niu, W.; Graham, J. O.; DuChene, J. S.; Qiu, J.; Wang, Y. C.; Engelhard, M. H.; Su, D.; Stach, E. A.; Wei, W. D. Surface Plasmon-Driven Water Reduction: Gold Nanoparticle Size Matters. *J. Am. Chem. Soc.* **2014**, *136*, 9842−9845.

(15) Valden, M.; Lai, X.; Goodman, D. W. Onset of Catalytic Activity of Gold Clusters on Titania with the Appearance. *Science* **1998**, *281*, 1647−1650.

(16) Herzing, A. A.; Kiely, C. J.; Carley, A. F.; Landon, P.; Hutchings, G. J. Identification of Active Gold Nanoclusters on Iron Oxide Supports for CO Oxidation. *Science* **2008**, *321*, 1331−1335.

(17) Kibria, M. G.; Chowdhury, F. A.; Zhao, S.; AlOtaibi, B.; Trudeau, M. L.; Guo, H.; Mi, Z. Visible Light-Driven Efficient Overall Water Splitting Using P-type Metal-Nitride Nanowire Arrays. *Nat. Commun.* **2015**, *6*, 6797.

(18) Mubeen, S.; Lee, J.; Singh, N.; Kramer, S.; Stucky, G. D.; Moskovits, M. An Autonomous Photosynthetic Device in Which All Charge Carriers Derive from Surface Plasmons. *Nat. Nanotechnol.* **2013**, *8*, 247−251.

(19) Chen, H. M.; Chen, C. K.; Chen, C. J.; Cheng, L. C.; Wu, P. C.; Cheng, B. H.; Ho, Y. Z.; Tseng, M. L.; Hsu, Y. Y.; Chan, T. S.; Lee, J. F.; Liu, R. S.; Tsai, D. P. Plasmon Inducing Effects for Enhanced Photoelectrochemical Water Splitting: X-ray Absorption Approach to Electronic Structures. *ACS Nano* **2012**, *6*, 7362−7372.

(20) Robatjazi, H.; Bahauddin, S. M.; Doiron, C.; Thomann, I. Direct Plasmon-Driven Photoelectrocatalysis. *Nano Lett.* **2015**, *15*, 6155−6161.

(21) Zhang, H.; Alexander, O. G. Optical Generation of Hot Plasmonic Carriers in Metal Nanocrystals: the Effects of Shape and Field Enhancement. *J. Phys. Chem. C* **2014**, *118*, 7606−7614.

(22) Long, R.; Prezhdo, O. V. Instantaneous Generation of Charge-Separated State on TiO_2 Surface Sensitized with Plasmonic Nanoparticles. *J. Am. Chem. Soc.* **2014**, *136*, 4343−4354.

(23) Cottancin, E.; Celep, G.; Lermé, J.; Pellarin, M.; Huntzinger, J. R.; Vialle, J. L.; Broyer, M. Optical Properties of Noble Metal Clusters as a Function of the Size: Comparison between Experiments and a Semi-Quantal Theory. *Theor. Chem. Acc.* **2006**, *116*, 514−523.

(24) Kale, M. J.; Avanesian, T.; Christopher, P. Direct Photocatalysis by Plasmonic Nanostructures. *ACS Catal.* **2014**, *4*, 116−128.

(25) Christopher, P.; Xin, H.; Linic, S. Visible-Light-Enhanced Catalytic Oxidation Reactions on Plasmonic Silver Nanostructures. *Nat. Chem.* **2011**, *3*, 467−472.

DOI: 10.1021/acsnano.6b01840
ACS Nano 2016, 10, 5452−5458

(26) Yan, L.; Ding, Z.; Song, P.; Wang, F.; Meng, S. Plasmon-Induced Dynamics of H_2 Splitting on a Silver Atomic Chain. *Appl. Phys. Lett.* **2015**, *107*, 083102.
(27) Gao, S. Nonlinear Response of Metal Nanoparticles: Double Plasmon Excitation and Electron Transfer. *J. Chem. Phys.* **2015**, *142*, 234701.
(28) Zhu, M.; Aikens, C. M.; Hollander, F. J.; Schatz, G. C.; Jin, R. Correlating the Crystal Structure of a Thiol-Protected Au_{25} Cluster and Optical Properties. *J. Am. Chem. Soc.* **2008**, *130*, 5883−5885.
(29) Scholl, J. A.; Koh, A. L.; Dionne, J. A. Quantum Plasmon Resonances of Individual Metallic Nanoparticles. *Nature* **2012**, *483*, 421−427.
(30) Yan, J.; Jacobsen, K. W.; Thygesen, K. S. First-Principles Study of Surface Plasmons on Ag(111) and H/Ag(111). *Phys. Rev. B: Condens. Matter Mater. Phys.* **2011**, *84*, 235430.
(31) Kale, M. J.; Avanesian, T.; Xin, H.; Yan, J.; Christopher, P. Controlling Catalytic Selectivity on Metal Nanoparticles by Direct Photoexcitation of Adsorbate−Metal Bonds. *Nano Lett.* **2014**, *14*, 5405−5412.
(32) Zhou, L.; Zhang, C.; McClain, M. J.; Manjavacas, A.; Krauter, C. M.; Tian, S.; Berg, F.; Everitt, H. O.; Carter, E. A.; Nordlander, P.; Halas, N. J. Aluminum Nanocrystals as a Plasmonic Photocatalyst for Hydrogen Dissociation. *Nano Lett.* **2016**, *16*, 1478−1484.
(33) Townsend, E.; Bryant, G. W. Which Resonances in Small Metallic Nanoparticles Are Plasmonic? *J. Opt.* **2014**, *16*, 114022.
(34) Townsend, E.; Bryant, G. W. Plasmonic Properties of Metallic Nanoparticles: the Effects of Size Quantization. *Nano Lett.* **2012**, *12*, 429−434.
(35) Ma, J.; Wang, Z.; Wang, L. W. Interplay between Plasmon and Single-Particle Excitations in a Metal Nanocluster. *Nat. Commun.* **2015**, *6*, 10107.
(36) Toker, G.; Bespaly, A.; Zilberberg, L.; Asscher, M. Enhanced Photochemistry of Ethyl Chloride on Ag Nanoparticles. *Nano Lett.* **2015**, *15*, 936−942.
(37) Kale, M. J.; Christopher, P. Plasmons at the Interface. *Science* **2015**, *349*, 587−588.
(38) Dodekatos, G.; Schuenemann, S.; Tueysuez, H. Surface Plasmon-Assisted Solar Energy Conversion. *Top. Curr. Chem.* **2015**, *371*, 215−252.
(39) Bauer, C.; Abid, J. P.; Fermin, D.; Girault, H. H. Ultrafast Chemical Interface Scattering as an Additional Decay Channel for Nascent Nonthermal Electrons in Small Metal Nanoparticles. *J. Chem. Phys.* **2004**, *120*, 9302−9315.
(40) Linic, S.; Aslam, U.; Boerigter, C.; Morabito, M. Photochemical Transformations on Plasmonic Metal Nanoparticles. *Nat. Mater.* **2015**, *14*, 567−576.
(41) Boerigter, C.; Campana, R.; Morabito, M.; Linic, S. Evidence and Implications of Direct Charge Excitation as the Dominant Mechanism in Plasmon-Mediated Photocatalysis. *Nat. Commun.* **2016**, *7*, 10545.
(42) Wu, K.; Chen, J.; McBride, J. R.; Lian, T. Efficient Hot-electron Transfer by a Plasmon-Induced Interfacial Charge-Transfer Transition. *Science* **2015**, *349*, 632−635.
(43) Castro, A.; Appel, H.; Oliveira, M.; Rozzi, C. A.; Andrade, X.; Lorenzen, F.; Marques, M.; Gross, E.; Rubio, A. Octopus: a Tool for the Application of Time-Dependent Density Functional Theory. *Phys. Status Solidi B* **2006**, *243*, 2465−2488.
(44) Zuloaga, J.; Prodan, E.; Nordlander, P. Quantum Description of the Plasmon Resonances of a Nanoparticle Dimer. *Nano Lett.* **2009**, *9*, 887−891.
(45) Prodan, E.; Nordlander, P. Structural Tunability of the Plasmon Resonances in Metallic Nanoshells. *Nano Lett.* **2003**, *3*, 543−547.
(46) Zheng, J.; Zhang, C.; Dickson, R. M. Highly Fluorescent, Water-Soluble, Size-Tunable Gold Quantum Dots. *Phys. Rev. Lett.* **2004**, *93*, 077402.
(47) Manjavacas, A.; Liu, J. G.; Kulkarni, V.; Nordlander, P. Plasmon-Induced Hot Carriers in Metallic Nanoparticles. *ACS Nano* **2014**, *8*, 7630−7638.
(48) Troullier, N.; Martins, J. L. Efficient Pseudopotentials for Plane-Wave Calculation. *Phys. Rev. B: Condens. Matter Mater. Phys.* **1991**, *43*, 1993−2006.
(49) Ceperley, D. M.; Alder, B. J. Ground State of the Electron Gas by a Stochastic Method. *Phys. Rev. Lett.* **1980**, *45*, 566.
(50) Alonso, J. L.; Andrade, X.; Echenique, P.; Falceto, F.; Prada-Gracia, D.; Rubio, A. Efficient Formalism for Large-Scale *Ab Initio* Molecular Dynamics Based on Time-Dependent Density Functional Theory. *Phys. Rev. Lett.* **2008**, *101*, 096403.
(51) Castro, A.; Marques, M. A. L.; Rubio, A. Propagators for the Time-Dependent Kohn-Sham Equations. *J. Chem. Phys.* **2004**, *121*, 3425−3433.
(52) Yan, J.; Yuan, Z.; Gao, S. W. End and Central Plasmon Resonances in Linear Atomic Chains. *Phys. Rev. Lett.* **2007**, *98*, 216602.
(53) Ding, Z. J.; Meng, S. Promote Water Photosplitting *via* Tuning Quantum Well States in Supported Metal Clusters. *Phys. Rev. B: Condens. Matter Mater. Phys.* **2012**, *86*, 045455.
(54) Mårsell, E.; Losquin, A.; Svärd, R.; Miranda, M.; Guo, C.; Harth, A.; Lorek, E.; Mauritsson, J.; Arnold, C. L.; Xu, H.; Huillier, A. L.; Mikkelsen, A. Nanoscale Imaging of Local Few-Femtosecond Near-Field Dynamics within a Single Plasmonic Nanoantenna. *Nano Lett.* **2015**, *15*, 6601−6608.

DOI: 10.1021/acsnano.6b01840
ACS Nano 2016, 10, 5452−5458